J. Fluid Mech. (1982), *vol.* 118, *pp.* 143–164
Printed in Great Britain

The response of a turbulent boundary layer to a short length of surface roughness

By J. ANDREOPOULOS
Sonderforschungsbereich 80, Universität Karlsruhe, W. Germany
AND D. H. WOOD†
Department of Aeronautics, Imperial College, London, U.K.

(Received 6 October 1980 and in revised form 6 October 1981)

Extensive measurements were made of the response of a high-Reynolds-number turbulent boundary layer to a short length (about three boundary-layer thicknesses) of surface roughness. The measurements include the mean velocity, all the Reynolds streses as well as all the triple products occurring in the Reynolds-stress transport equations. At the last measurement station, 55 boundary-layer thicknesses from the roughness, the boundary layer still had not relaxed to the universal smooth-wall structure. Comparison of the measurements with a calculation of the flow suggests the major requirement for improving the agreement is a more sophisticated treatment of the turbulent-diffusion process.

1. Introduction

The wall region of a turbulent boundary layer is one of the simplest regions of turbulent shear flow to calculate because the *equilibrium* structure, from which the logarithmic mean-velocity profile follows, is determined almost entirely by the *local* processes of turbulent-energy production and dissipation (Townsend 1961). Present-day calculation methods are reasonably capable of describing the response of the wall region to a large step change in surface roughness, that is from one equilibrium flow to another, even though the flow immediately following the step is not in energy equilibrium (Wood 1978).

The outer region ($y/\delta \gtrsim 0{\cdot}2$, where δ is the boundary-layer thickness) is more complex, as its time scales are much larger than in the wall region owing to the importance of non-local effects, such as the diffusion and advection of turbulent energy. Most calculation methods generally succeed only in regions far removed from any strong perturbation, hereinafter called a self-preserving flow to emphasize the difference from equilibrium as defined above; the latter is a subset of the former. Antonia & Luxton (1971*a*, 1972) found that the whole flow had adjusted to a large smooth-to-rough step (hereinafter denoted $S \rightarrow R$) by a streamwise distance of about $10\delta_0$, where δ_0 is the initial boundary-layer thickness defined in figure 1. However, recovery following a rough-to-smooth step ($R \rightarrow S$)‡ was far from complete by their last measuring station, $x/\delta_0 = 16$.

† Present address: Department of Mechanical Engineering, University of Newcastle, N.S.W., Australia.

‡ We use the abbreviations $S \rightarrow R$ and $R \rightarrow S$ with the implication that they describe the transition from one self-preserving flow to another.

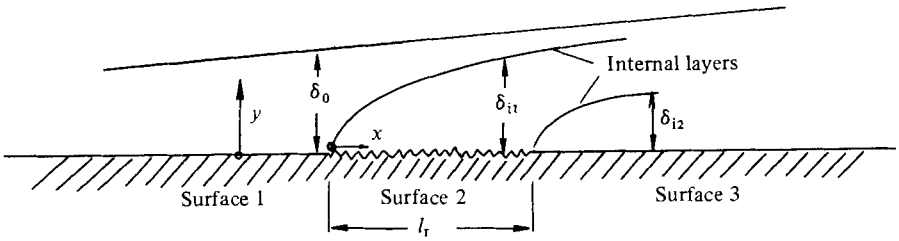

FIGURE 1. Schematic diagram of the flow.

The major aim of the present equipment is to document further the recovery of the outer layer to a change in the wall boundary condition. Since the response length of the outer layer is roughly $10\delta_0$ (Smits, Young & Bradshaw 1979) we decided to measure the flow following an 'impulse' of surface roughness whose length was arbitrarily set at around $3\delta_0$. This geometry had the added advantage that the wall-region flow was not in equilibrium at the end of the roughness strip, providing a more difficult test case for calculation methods than previous, single-step experiments. The experiment is an idealization of important micrometeorological flows and also those in which corrosion or erosion alter the surface over a short distance as might occur in river beds or on turbine blades.

The experiment is shown schematically in figure 1. A fully developed turbulent boundary layer has formed on the upstream surface. At $x = 0$ the surface roughness changes abruptly by an amount that is usually measured as $M \equiv \ln z_{01}/z_{02}$; the roughness scale z_0 is obtained by writing the logarithmic law as $U/U_\tau = \kappa^{-1} \ln (y/z_0)$, where U is the mean streamwise velocity, U_τ is the friction velocity and κ is the Kármán constant ($\simeq 0{\cdot}41$, the value that has been used here throughout the present study). The flow adjusts by forming an internal layer whose height δ_{i1} denotes the outward extent of the velocity field affected by the new surface, since streamline displacement effects are small (see e.g. Antonia & Luxton (1971*a*, 1972)). At $l_r = 150\,\text{mm}$ ($\simeq 3\delta_0$) a second step change in roughness occurs before the flow has fully adjusted to the new surface. A second internal layer with height δ_{i2} is formed under the high mean-velocity gradient $\partial U/\partial y$ caused by the first step.

Two important problems occur in measuring the flow over a rough surface. Firstly, it is difficult to estimate the wall shear stress accurately, and, secondly, the origin for the normal co-ordinate y is not known *a priori*. These problems increase the uncertainty of fitting the mean-velocity profiles to the logarithmic law, even for fully developed flow. Andreopoulos & Bradshaw (1981) found that roughness effects on the structure of a fully developed boundary layer are small when normalized by U_τ and δ, although the triple products appearing in the turbulent-energy equation are altered spectacularly up to ten physical roughness heights from the surface.

The experimental results include all the measurable terms appearing in the Reynolds-stress transport equations. They leave no doubt that the flow has not recovered to its usual smooth-wall self-preserving form at the last measurement station, $x/\delta_0 = 55$.

The measurement techniques are described briefly in §2, while §3 presents and discusses a selection of the results; more details are available in Andreopoulos (1979) and Andreopoulos & Wood (1980), where the hot-wire results are tabulated. Calculations made using the Bradshaw, Ferriss & Atwell (1967) method are compared with

the measurements in §4. It is suggested that the main requirement for improving the accuracy of calculations in general is an improved modelling of the triple-product terms in the Reynolds-stress equations.

2. Experimental techniques and data reduction

The measurements were made in the closed-circuit wind tunnel at the Sonderforschungsbereich 80, which has a 6 m long by 1·5 m internal diameter octagonally shaped working section, with an adjustable roof set to give a zero pressure gradient. The free-stream longitudinal intensity was about 0·06 % at 14 m s^{-1}; further details of the tunnel's performance are given by Ermshaus & Naudascher (1977). A 6 m long flat plate was installed 30 cm from the floor. A flap installed at the trailing edge was adjusted to give zero circulation around the plate. To avoid low-Reynolds-number effects, and in the naive belief that there would remain sufficient streamwise distance for complete recovery, a sandpaper strip of 150 mm was installed about 2·95 m from the leading edge. The roughness was not closely packed and had a maximum grain size of about 2 mm with a backing thickness of 1 mm. The plate was machined to accept the strip with the top of the backing just below the plate surface, so the roughness was slightly upstanding.

At constant height within the boundary layer the mean velocity was uniform over the central 85 % of the plate at 3 m from the leading edge. Similarly, $\overline{u^2}$ was effectively invariant with spanwise position over 75 % of the plate width at 4·5 m from the leading edge.

Both the mean velocity and turbulence structure of the boundary layer upstream of the step were found to be close to those for a standard smooth-wall, zero-pressure-gradient layer (Andreopoulos 1980). Low-Reynolds-number effects are negligible (table 1) and the free-stream velocity U_e was always maintained to within $\pm 0{\cdot}5$ % of 14·75 m s^{-1}.

The streamwise mean velocity was measured with a round-total head tube of 1 mm outside diameter connected to a MKS Baratron Type 144 pressure transducer. Skin-friction measurements were made on the smooth wall using Preston tubes of 1 mm and 2 mm outside diameter and Patel's (1965) calibration.

DISA 55M01 constant-temperature anemometers were used for all the turbulence measurements. DISA 55P51 X-probes were used mainly, but some simultaneous measurements of all three velocity components were obtained using a DISA 55P91 three-wire probe. After low-pass filtering at 10 kHz the hot-wire signals were digitized at a rate of 5 kHz per channel by a Hewlett-Packard 5154C Fourier Analyser, and 20 s of real-time data were recorded on digital tape. The tapes, which are still available, were later analysed on the Univac 1108 computer of the University of Karlsruhe. The digitization system and the data-reduction program used to evaluate all the products up to third order as well as $\overline{u^4}$, $\overline{v^4}$ and $\overline{w^4}$ are described by Andreopoulos (1980). The X-probes were calibrated using King's law and a modified version of the 'cosine law' with the effective yaw angle obtained by calibration in the (x, y)-plane ((u, v)-plane). To measure u and w the probe was rotated 90° in the (y, z)-plane, while $\overline{w^2v}$ was determined from measurements at $\pm 45°$ in that plane. The data-reduction program simply inverted the calibrations, so no analogue linearization was necessary. The system allowed a large number of profiles to be measured quickly; and subsequent

recalibration of the probes showed virtually no drift from the calibrations for the results presented here. The calibration of the three-wire probe and its advantages and limitations are discussed in Andreopoulos (1981). The agreement between the X-probe and three-wire-probe results was very good and the results are presented in §3 without reference to the probes used.

3. Results

3.1. *Mean flow*

The mean-velocity data are tabulated in Andreopoulos (1979) and the bulk-flow parameters are summarized in table 1. Estimates of the skin-friction coefficient c_f are shown in figure 2 together with the calculations discussed in §4. The Clauser-chart values were obtained using the logarithmic law for a rough surface

$$\frac{U}{U_\tau} = \frac{1}{\kappa}\ln\frac{y+e}{\nu}U_\tau + A - \frac{\Delta U}{U_\tau}, \tag{3.1}$$

where A is the additive constant in the upstream smooth-wall logarithmic law. The error in origin e was found using the method of Perry, Schofield & Joubert (1969) to be nearly 1 mm above the smooth surface and independent of x for $x \leqslant 150$ mm (Andreopoulos 1979); obviously $e = 0$ for $x > 150$ mm. In that sense e is expected to vary discontinuously at $x = 150$ mm. The value of the roughness function, or velocity shift, $\Delta U/U_\tau$, then follows. Since both the Preston tube and Clauser chart depend on the applicability of the logarithmic law, and hence on the existence of equilibrium, they will be inaccurate close to a step change in roughness. Although there is significant disagreement between the results, as was found by Antonia & Luxton (1972) after a $R \rightarrow S$ step, both methods agree on the trend in c_f. In particular, dc_f/dx is negative only at the last measuring station. This is a requirement for fully developed flow, which must therefore occur after the last measuring station.

Another estimate of c_f comes from the momentum-integral equation $c_f = 2d\theta/dx$, where θ is the momentum thickness, and pressure-gradient effects are negligible. Because of the inevitable scatter, a smooth curve was passed through the results and c_f determined. Unfortunately, the method is also unreliable near a step where c_f has large streamwise gradients of both signs, but there is generally good agreement with the Clauser-chart values after the second step.

The reason for the disagreement between the Preston-tube and Clauser-chart values of c_f is evident from figure 3, which shows the streamwise development of $\Delta U/U_\tau$. Even at the last measuring station $\Delta U/U_\tau$ has not returned to its equilibrium smooth-wall value of zero; the present value of $\Delta U/U_\tau \simeq 2{\cdot}0$ is very close to that found by Antonia & Luxton (1972) at their last station. Since the calibration of the Preston tube requires that $\Delta U/U_\tau = 0$, the disagreement is not surprising, and suggests that the Clauser-chart values are more reliable. The slight decrease in c_f with decreasing outside diameter at all x is consistent with the lack of equilibrium in the wall region and with the viscous sublayer having its usual form $U^+ = y^+$, where $U^+ \equiv U/U_\tau$ and $y^+ \equiv yU_\tau/\nu$; the centre of the 1 mm outside diameter tube is at $y^+ \simeq 16$ for $c_f = 0{\cdot}0023$.

x (mm)	δ^* (mm)	H	θ (mm)	δ (mm)
−100·00	5·829	1·298	4·469	43·752
−10·00	6·206	1·299	4·777	44·882
0·00	5·979	1·271	4·665	46·666
10·00	5·476	1·273	4·302	44·412
50·00	5·950	1·337	4·447	46·683
100·00	6·797	1·362	4·990	46·005
137·50	6·305	1·358	4·642	48·566
150·00	6·847	1·357	5·045	50·027
176·00	8·106	1·493	5·465	46·814
200·00	7·607	1·434	5·441	47·673
225·00	7·926	1·432	5·535	48·477
250·00	8·279	1·408	5·877	51·532
350·00	8·267	1·381	5·997	52·900
650·00	8·469	1·341	6·314	55·551
1000·00	7·933	1·307	6·065	53·900
1750·00	8·792	1·298	6·770	60·165
2500·00	10·261	1·297	7·913	74·451

TABLE 1. Bulk-flow parameters. The largest contributions to θ comes from values of U/U_e around 0·5, as $U/U_e(1-U/U_e)$ has maximum value 0·25 at $U/U_e = 0{\cdot}5$. The smallest value of U/U_e was greater than 0·5 at $y = 0{\cdot}94$ mm; so θ and δ^* may not be reliable.

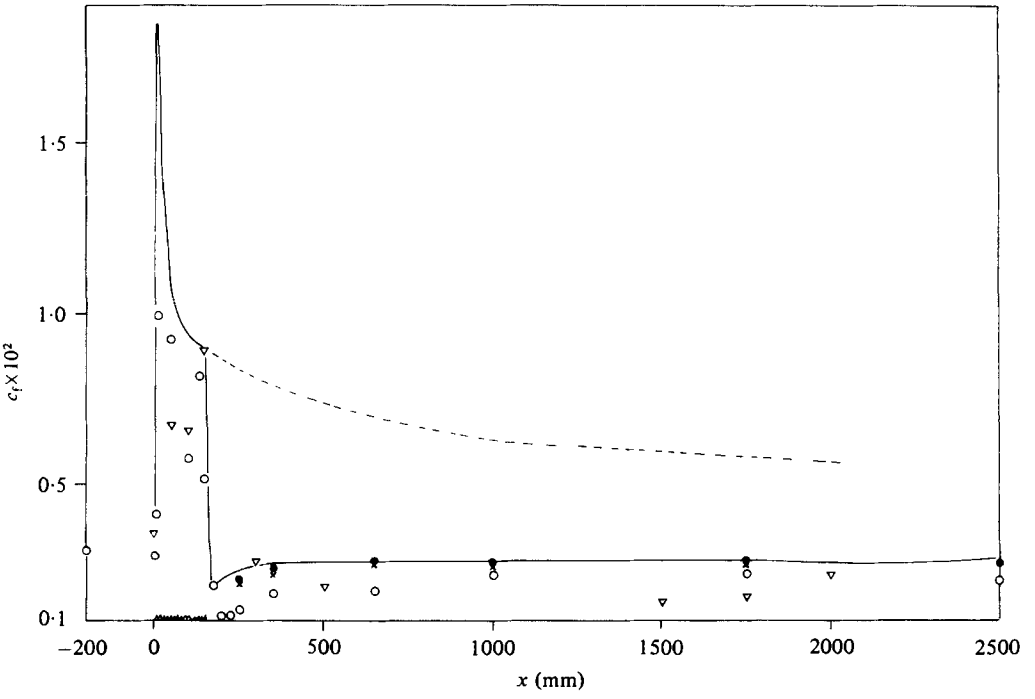

FIGURE 2. Development of the skin-friction coefficient. Solid line is the calculated development; ○, Clauser chart; ▽, momentum thickness; ●, ×, Preston tube of 1 and 2 mm outer diameter respectively.

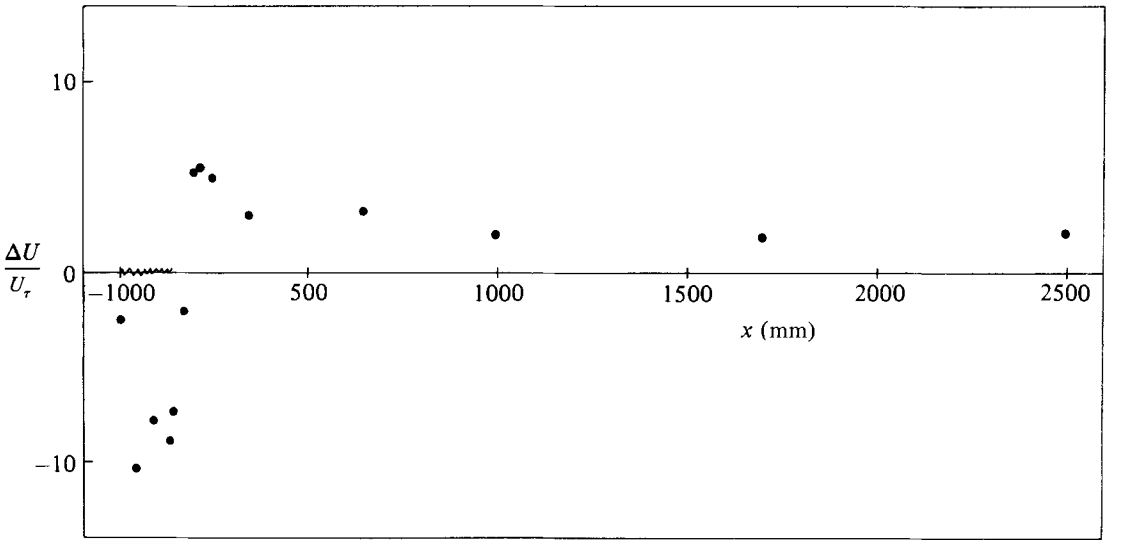

FIGURE 3. Development of $\Delta U/U_\tau$.

3.2. *Growth of the internal layers*

The height of the internal layer(s) was found as the point(s) at which successive mean velocity profiles merged. More precisely, mean longitudinal velocity gradients $\partial U/\partial x$ were compared with $\epsilon U_e/\delta$, where U_e is the free-stream velocity, δ the thickness of the outer layer and ϵ some suitably small number. The height of the internal layer is then defined as the distance y where

$$\frac{\partial U}{\partial x} \leqslant \frac{\epsilon U_e}{\delta}.$$

The value of ϵ must be as small as possible, but certainly greater than that allowed by the available accuracy of velocity measurements and the uncertainties involved in deducing the longitudinal gradients. Finally, ϵ has been set equal to 0·02, and it was found that the growth rate of the internal layer is independent of ϵ for a range of 40 % variation of ϵ. (Hereinafter ϵ will be used to denote the dissipation of turbulent kinetic energy.)

The striking difference in the growth rates of δ_{i1} and δ_{i2} is shown in figure 4. The first internal layer reaches the boundary-layer edge at about $x/\delta_0 = 13$, while even at the last station δ_{i2} has hardly penetrated the outer region.

On largely dimensional grounds, Wood (1980) showed that for single $S \rightarrow R$ and $R \rightarrow S$ steps the wall-region behaviour of δ_i could be correlated approximately as

$$\frac{\delta_i}{z_{01}} = f(M)\left(\frac{x}{z_{02}}\right)^{0\cdot8}. \tag{3.2}$$

For the present results

$$\frac{\delta_{i1}}{z_{01}} = 15\cdot68\left(\frac{x}{z_{02}}\right)^{0\cdot8} \tag{3.3}$$

over nearly all x/δ. There appear to be three overlapping regions for the second internal layer, given approximately by

$$\frac{\delta_{i2}}{z_{02}} = 0\cdot0078\left(\frac{x}{z_{03}}\right)^{0\cdot8} \quad (0 < x/\delta < 2), \tag{3.4}$$

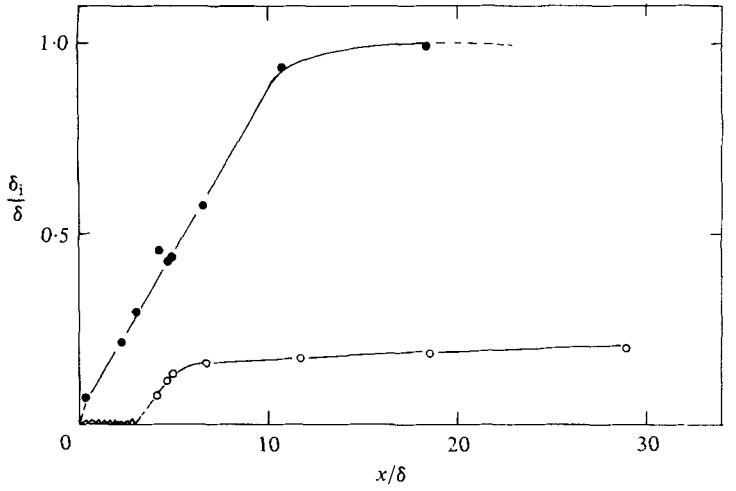

FIGURE 4. Development of the internal-layer thickness. ●, δ_{i1}/δ; ○, δ_{i2}/δ.

$$\frac{\delta_{i2}}{z_{02}} = 0{\cdot}069\left(\frac{x}{z_{03}}\right)^{0{\cdot}48} \quad (2 < x/\delta < 4), \tag{3.5}$$

$$\frac{\delta_{i2}}{z_{02}} = 0{\cdot}027\left(\frac{x}{z_{03}}\right)^{0{\cdot}2} \quad (4 < x/\delta). \tag{3.6}$$

The values of z_{01} and z_{03} were found by applying the equation for z_0 from the logarithmic law (3.1),

$$z_0 = \frac{\nu}{U_\tau}\exp[-\kappa C + \Delta U/U_\tau),$$

at $x = 0$, where $\Delta U/U_\tau = 0$, and at $x = 2500\,\text{mm}$, where $\Delta U/U_\tau = 2{\cdot}0$. The values obtained were $z_{01} = 3{\cdot}43 \times 10^{-3}\,\text{mm}$ and $z_{03} = 1{\cdot}74 \times 10^{-3}\,\text{mm}$. Again using (3.1), z_{02} was found to be approximately 0·134 mm. It is emphasized that both z_{02} and z_{03} are approximate, since they were not measured under equilibrium conditions. Using these values we find $M_{1\to2} = -3{\cdot}67$ and $M_{2\to3} = 4{\cdot}34$, compared with Antonia & Luxton's (1971*a*, 1972) values of $M_{S\to R} = -4{\cdot}6$ and $M_{R\to S} = 5{\cdot}8$, showing that the 'strengths' of the perturbations are weaker in the present flow.

The growth of the first internal layer does not appear to be influenced by the second. The exponents in (3.3) and (3.4) agree, while that in (3.5) is close to the value of 0·43 measured by Antonia & Luxton (1972) over a similar range of x/δ. Even though the errors in estimating δ_i are large in the outer layer where the perturbation is weak, (3.6) is further indication that the flow has not reached full development by the last station.

3.3. *Turbulence measurements*

Considerable thought was given to the problem of making the turbulence measurements non-dimensional. It is unlikely that U_τ is acceptable, because of the lack of equilibrium and because of the inaccuracy of estimating U_τ, at least close to the steps. However, figure 5 shows that even if U_τ is factored it is still impossible to collapse the shear stress over all y/δ at $x = 1750\,\text{mm}$ onto the upstream distribution, in agreement with the above conclusions about the lack of full development. In the interests of safety the results are normalized by U_e and δ.

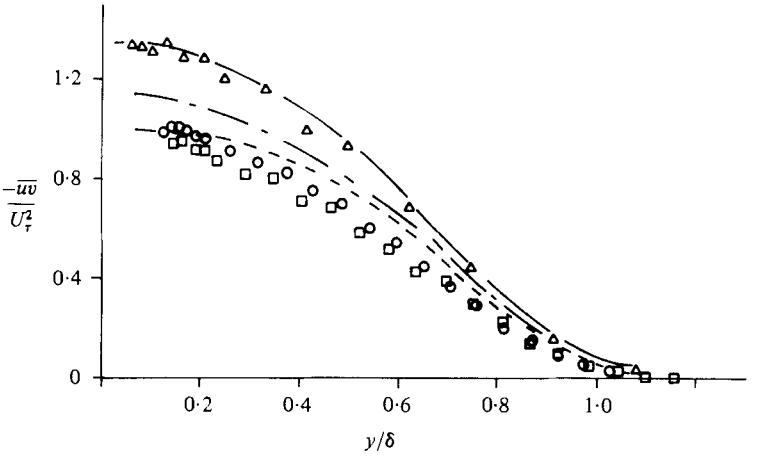

FIGURE 5. Shear-stress profiles scaled by U_τ^2. x (mm): □, −100; ○, 0; △, 1750. - - - -, U_τ increased by 25%; — - —, U_τ increased by 20%.

For $x < 150$ mm $\overline{u^2}$ (figure 6) and $\overline{v^2}$ (figure 7) are increased abruptly over their smooth-wall values for $y < \delta_{i}$, as a result of the sudden increase in $\partial U/\partial y$ and hence in turbulent-energy production. The shear stress $-\overline{uv}$ is also increased (figure 8), as its production, largely $\overline{v^2}\,\partial U/\partial y$, rises. The values of δ_{i1} and δ_{i2} from figure 4 are replotted in figure 8. For $x < 150$ mm, δ_{i1} is in reasonable agreement with the value obtained by superimposing successive $\overline{u^2}$, $\overline{v^2}$ or $-\overline{uv}$ profiles, as found by Antonia & Luxton (1971*a*). The initial rapid rise in the second-order quantities has finished by $x = 150$ mm; however, the maximum values of all the second-order quantities at $x = 175$ mm are between 5 to 7% higher than at 150 mm, as $\partial U/\partial y$ has also increased for $\delta_{i2} < y < \delta_{i1}$ ($\overline{w^2}$ is shown in figure 9). This does not occur in the single $R \rightarrow S$ measurements of Antonia & Luxton (1972). Furthermore, for $x = 200$ mm, and probably for 175 mm as well, the maxima in the second-order quantities occur significantly outside the second internal layer at about $y/\delta = 0{\cdot}11$ for $x = 200$ mm and not at $y = \delta_{i2}$ ($\delta_{i2}/\delta = 0{\cdot}075$), as would be the case if the flow was a simple superposition of a $S \rightarrow R$ followed quickly by a $R \rightarrow S$ step. The Clauser-chart values of U_τ^2 are indicated on the vertical axes in figure 8, showing that extrapolating $-\overline{uv}$ to the wall to estimate U_τ^2 is inherently unreliable. Within the second internal layer $-\overline{uv}$ is always larger than U_τ^2. It is worth noting that the $\overline{w^2}$ results (figure 9) do not support the approximation $\overline{w^2} \simeq \frac{1}{2}(\overline{u^2}+\overline{v^2})$ that has been widely used in the past when only u, v measurements were available.

The most obvious feature of figure 8 is the outward propagation of the peak in $-\overline{uv}$, which is not so evident in Antonia & Luxton's (1972) single-step results, since their $-\overline{uv}$ profile at the $R \rightarrow S$ step had the same shape as the present profile at $x = 0$. The present results for $x > 150$ mm are qualitatively very similar to those of Smits *et al.* (1979, figure 10*d*) following an 'impulse' of convex curvature. They called this phenomenon a 'stress bore', and noted that it propagates because the large negative $\partial(-\overline{uv})/\partial y$ on the free-stream side of the peak decelerates the flow (see their equation (1)), hence increasing production and outward propagation. However, the detailed mechanics of the bore is a 'result of turbulent transport *and* of interaction between the turbulence and the mean flow', whereas a reasonable description of the wall region following a single step can ignore the former mechanism (Wood 1978, 1980). The stress bore is discussed further in § 3.5.

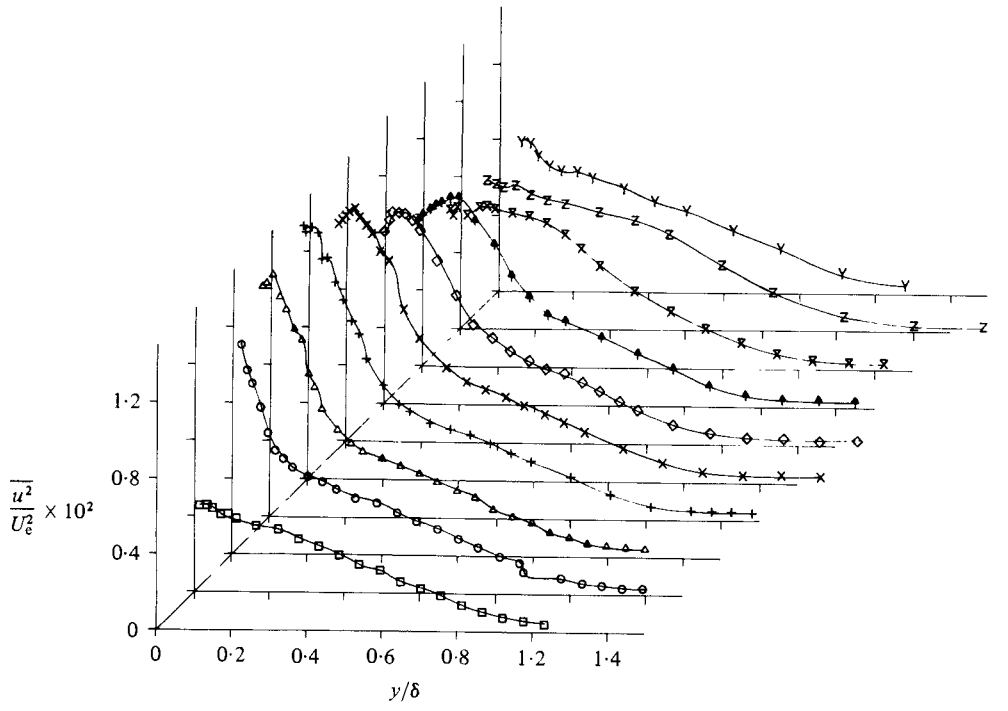

FIGURE 6. Mean-square u-profiles. x (mm): □, 0; ○, 100; △, 150; +, 175; ×, 200; ◇, 250; ▲, 300; ⧖, 500; Z, 1000; Y, 1750.

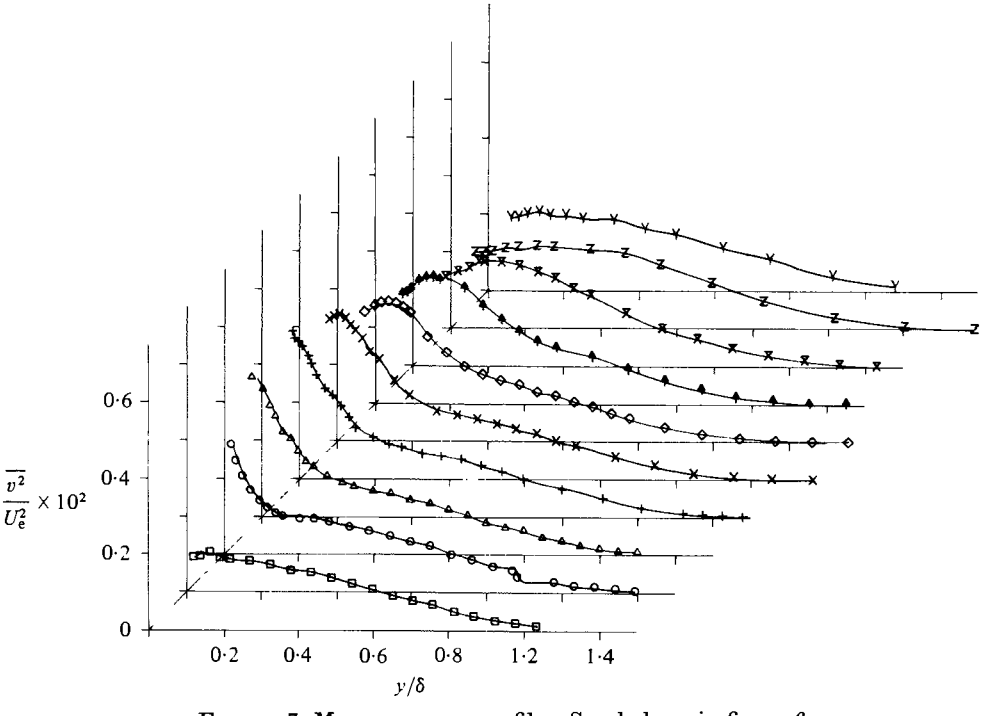

FIGURE 7. Mean-square v-profiles. Symbols as in figure 6.

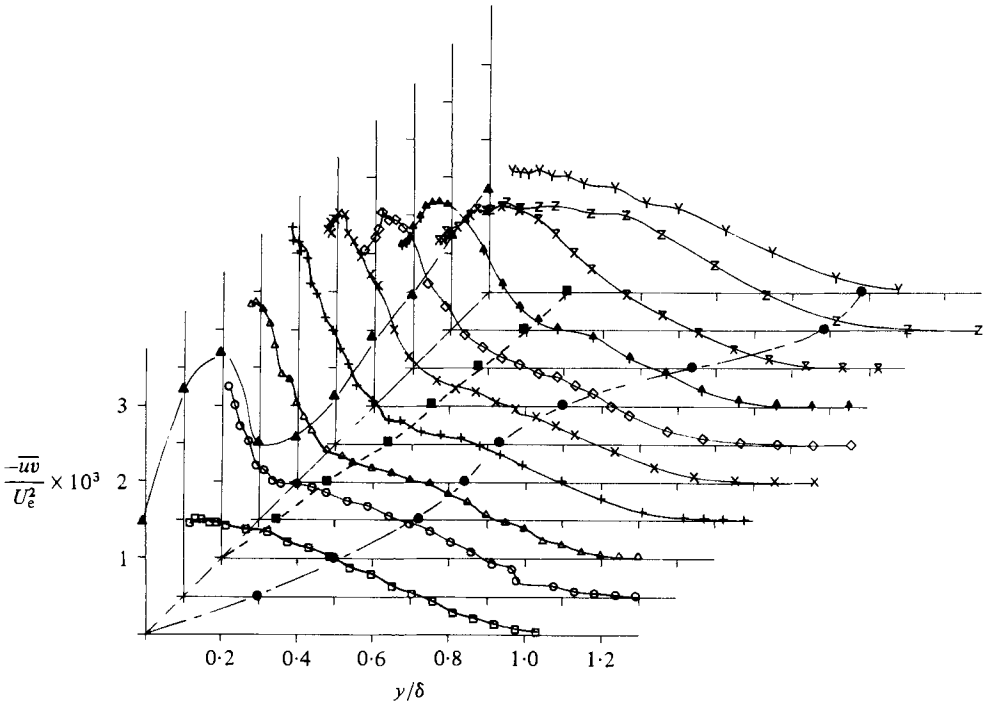

FIGURE 8. Shear-stress profiles. Symbols as in figure 6 and:
▲, Clauser-chart $\frac{1}{2}c_f$; ●, δ_{11}/δ; ■, δ_{12}/δ.

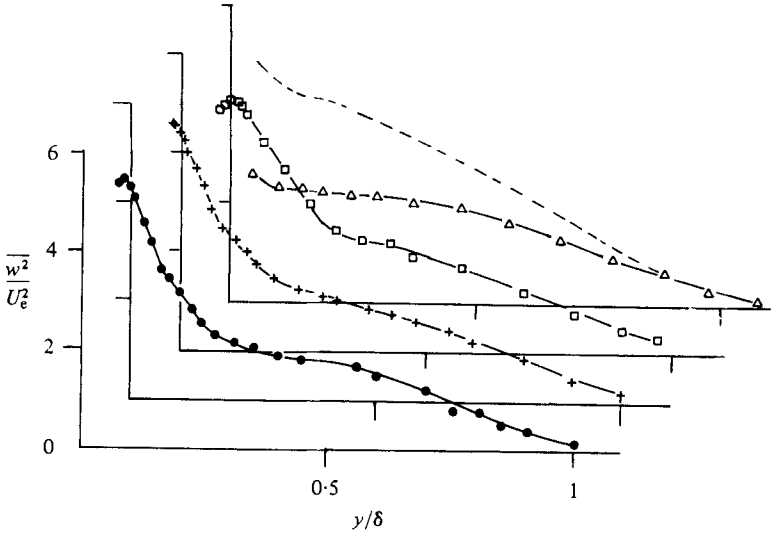

FIGURE 9. Mean-square w-profiles. x (mm), ●, 150; +, 175; □, 200; △, 1750.
- - - - line is $\frac{1}{2}(\overline{u^2}+\overline{v^2})$ at $x = 1750$.

The shear-stress correlation coefficient $R_{uv} \equiv -\overline{uv}/(\overline{u^2})^{\frac{1}{2}}(\overline{v^2})^{\frac{1}{2}}$ is plotted in figure 10. Its behaviour outside the first internal layer is unremarkable. For $x > 150$ mm, R_{uv} first increases, as $-\overline{uv}$ initially increases more rapidly than $\overline{u^2}$ and $\overline{v^2}$, and then decays more slowly. Between $x = 1000$ mm and 1750 mm, $-\overline{uv}$ remains nearly constant,

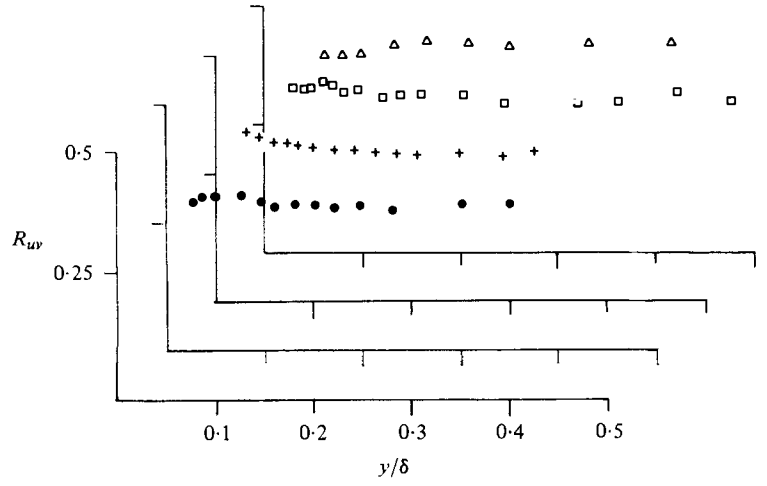

FIGURE 10. Shear–stress correlation coefficient. Symbols as in figure 9.

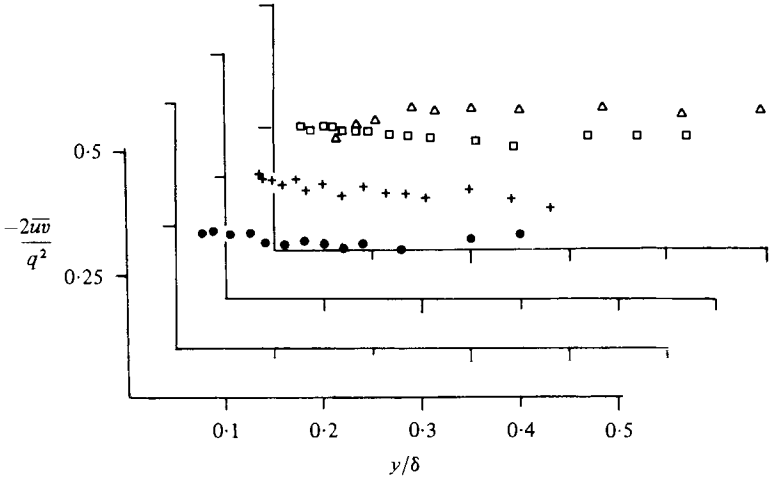

FIGURE 11. Structural parameter a_1. Symbols as in figure 9.

while $\overline{u^2}$ and $\overline{v^2}$ increase slightly. The behaviour of Townsend's (1961) structural parameter $a_1 \equiv -2uv/q^2$, where $q^2 = u^2+v^2+w^2$, behaves in a similar manner (figure 11). At $x = 150$ mm, a_1 has a maximum value within δ_{i1} of 0·32, while at $x = 175$ mm, the maximum measured value is 0·36. The departures from the value of 0·30 used in the calculation method of Bradshaw *et al.* (1967) are not large.

3.4. *Triple products*

The triple products are best described in terms of their contribution to the Reynolds-stress transport equations and by the resulting convection velocities for the Reynolds stresses. Before doing that, we briefly describe some important features of the results.

The measurements of $-\overline{u^3}$, $\overline{u^2v}$ and $\overline{v^3}$ are shown in figures 12–14. As expected, the large excursions from the fully developed smooth-wall values (at $x = 0$) are confined to $y < \delta_{i1}$. There, the resulting gradients of $\overline{u^2v}$ and $\overline{v^3}$ that appear in the turbulent-diffusion term for the turbulent energy have large values. For $x < 150$ mm the triple

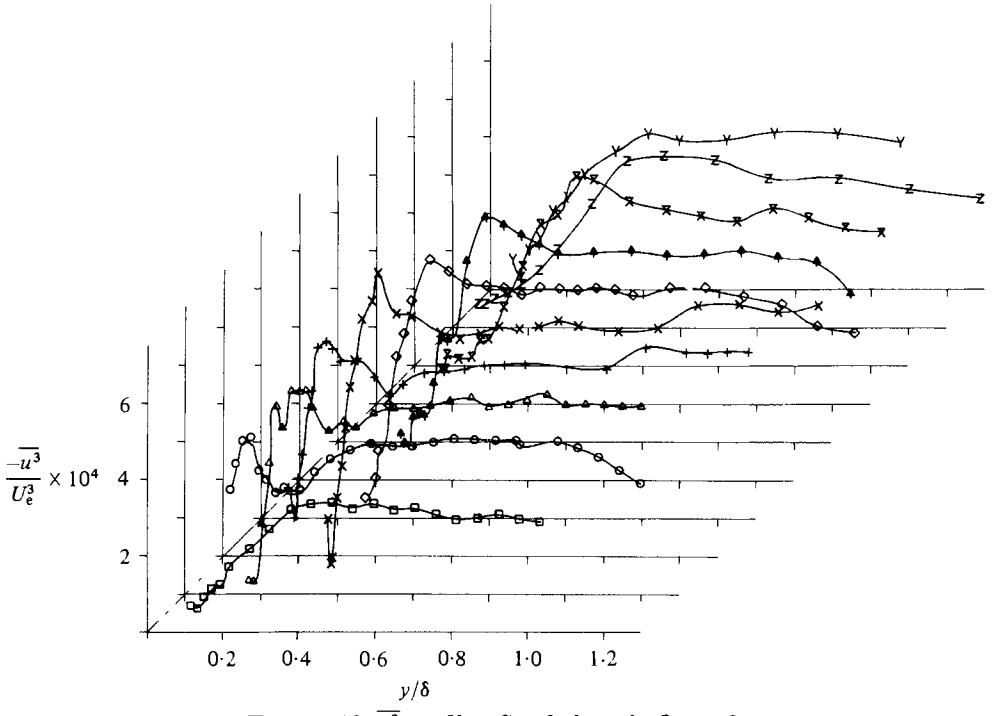

FIGURE 12. $\overline{u^3}$ profiles. Symbols as in figure 6.

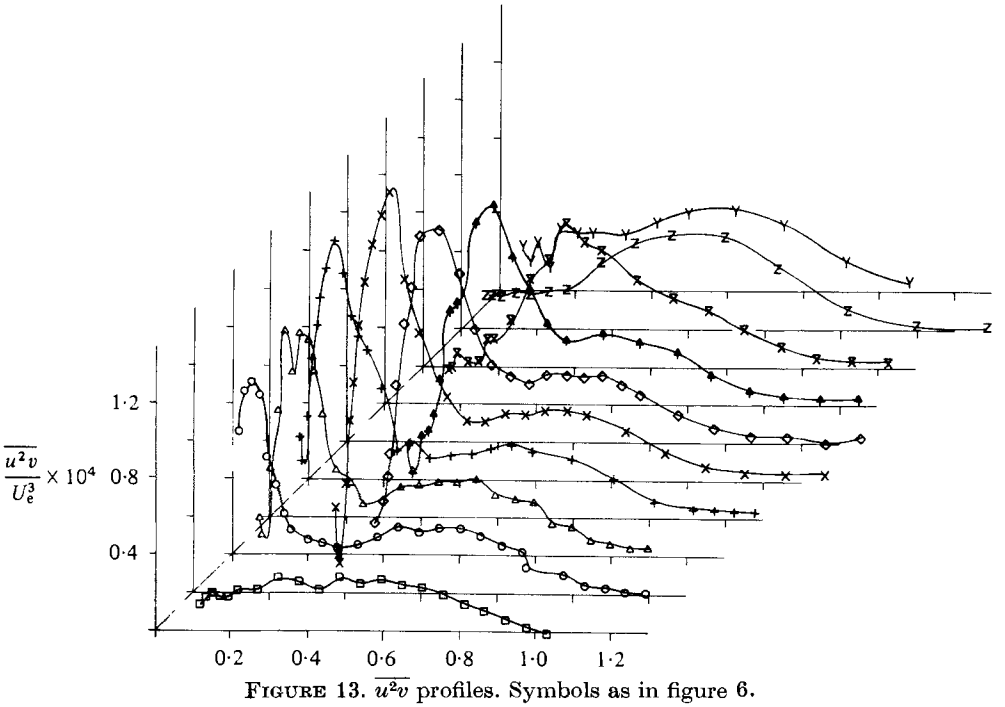

FIGURE 13. $\overline{u^2v}$ profiles. Symbols as in figure 6.

products peak towards the outer edge of the first internal layer, in substantial agreement with the finding of Antonia & Luxton (1974) that the skewness factors of u and v ($S_u \equiv \overline{u^3}/(\overline{u^2})^{\frac{3}{2}}$) are at maxima near $y/\delta_{i1} = 1$. They attributed this result to the

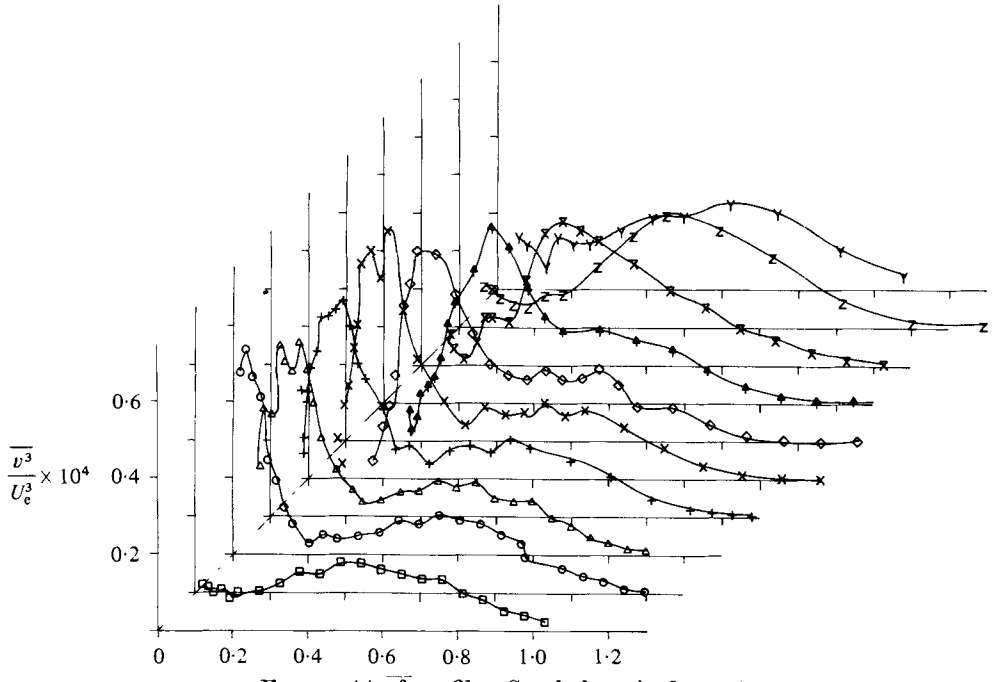

FIGURE 14. $\overline{v^3}$ profiles. Symbols as in figure 6.

flow 'switching' between the more intense rough-wall turbulence and the external flow. But this behaviour is also necessary for $\overline{u^2v}$ and $\overline{v^3}$, from the constraint on turbulent diffusion within δ_{i1} discussed in §3.5.

Close to the wall, $-\overline{u^3}$ develops a sharp negative peak for $x > 150$ mm similar to that found by Andreopoulos & Bradshaw (1980) for fully developed flow over both rough and smooth walls. In figure 12 the peak decays with x, and for $x > 150$ mm, $-\overline{u^3}$ is always positive. This difference from fully developed behaviour for large x also occurs for $\overline{u^2v}$.† Andreopoulos & Bradshaw (1980) found a negative peak in $\overline{v^3}$ close to the wall only for their fully developed rough flow. The present $\overline{v^3}$ results show a negative region for $y < \delta_{i2}$ and $x > 250$ mm, which has decayed only at the last station. The resulting large $\partial\overline{v^3}/\partial y$ contributes significantly to the turbulent diffusion.

Antonia & Luxton's (1972) results for $\overline{q^2v}$, which they assumed equal to $\frac{3}{2}(\overline{u^2v} + \overline{v^3})$ since $\overline{w^2v}$ was not measured, are always positive, whereas both $\overline{u^2v}$ and $\overline{v^3}$ are negative together at $x = 250$ and 300 mm.

3.5. *Reynolds-stress transport equations*

Figures 15–17 show the balance of the terms in the turbulent-energy equation

$$\left(U\frac{\partial}{\partial x} + V\frac{\partial}{\partial y}\right)\tfrac{1}{2}\overline{q^2} + \overline{uv}\frac{\partial U}{\partial y} + (\overline{u^2} - \overline{v^2})\frac{\partial U}{\partial x} + \frac{\partial}{\partial y}(\overline{pv} + \tfrac{1}{2}\overline{q^2v}) + \epsilon = 0,$$

that is

$$\text{advection} + \begin{matrix}\text{shear-}\\\text{stress}\\\text{production}\end{matrix} + \begin{matrix}\text{normal-}\\\text{stress}\\\text{production}\end{matrix} + \text{turbulent diffusion} + \text{dissipation} = 0,$$

† These conclusions are based on the assumption that the negative regions of $-\overline{u^3}$ and $\overline{u^2v}$ at $x = 0$ occurred closer to the wall than could be measured.

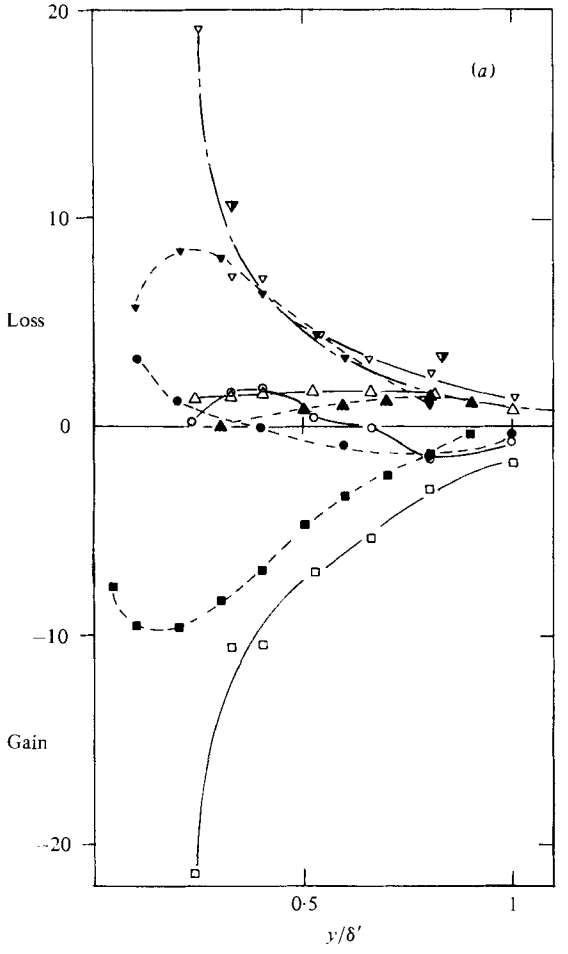

FIGURE 15 (*a*). For caption see opposite page.

for $x = 150$, 175 and 200 mm, where p is the fluctuating static pressure and the longitudinal diffusion was found to be small. As mentioned above all the turbulence terms except $\overline{pv}$ and ϵ were measured directly, the former was ignored and the latter found by difference. A rough check on the accuracy of the estimate for dissipation was made at a limited number of points by analysis of the spectra of u. In the inertial subrange $\phi_{uu} = a\epsilon^{\frac{2}{3}}k^{-\frac{5}{3}}$, where ϕ_{uu} is the one-dimensional spectral density of u, a is supposed to be a universal constant, taken here to be 0·50, and k is the streamwise wavenumber. Considering the combination of experimental error and the difficulties of graphical differentiation the agreement is satisfactory. In fact some of the discrepancy can be associated with the uncertainty in the value of a; Townsend (1976, p. 99) estimates this as $\pm 6\,\%$. The normal-stress production was always less than 4 % of the shear-stress production, with the maxima occurring close to the wall.

For a general comparison, the results at $x = 150$ mm, scaled by U_τ and δ_{i1}, are compared with the fully developed rough-wall results of Antonia & Luxton (1971*b*), scaled on U_τ and δ', in figure 15 (*a*). Surprisingly the present dissipation results are in better agreement with the equilibrium relation $\epsilon = U_\tau^3/\kappa y$, although this may be

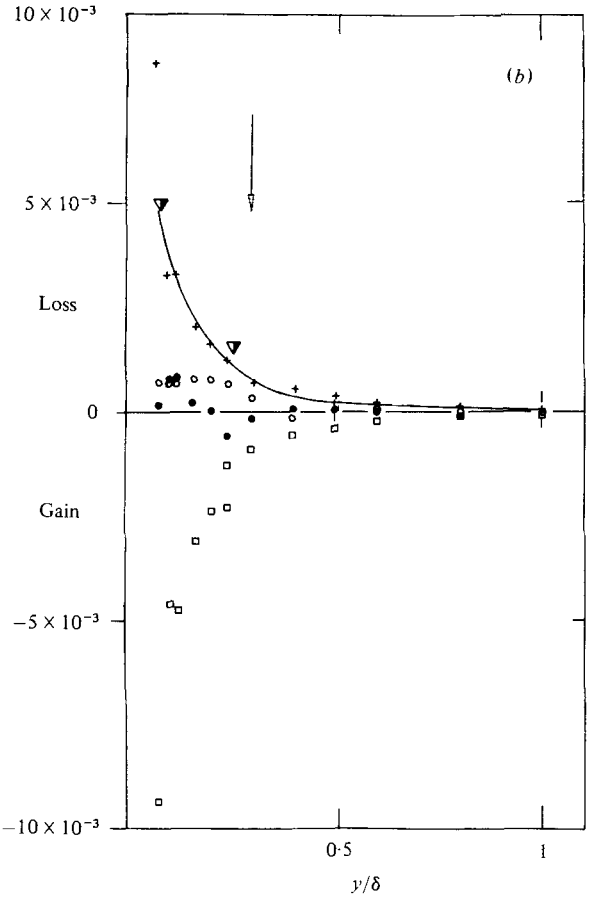

FIGURE 15. (*a*) Turbulent-energy balance at $x = 150$ mm scaled by U_τ and δ'; $\delta' = \delta_{i1}$ for present results and $\delta' = \delta$ for Antonia & Luxton (1971*b*, filled symbols). □, production; ▽, dissipation by difference; ▼, dissipation from spectral inertial subrange; — - —, equilibrium dissipation; △, advection; ○, diffusion. (*b*) Turbulent-energy balance at $x = 150$ mm, scaled by U_e and δ. +, dissipation by difference; ●, diffusion; ○, advection. Other symbols as in (*a*).

coincidence given the uncertainty in the estimates of U_τ, and there is a corresponding large difference in the production. As would be expected, advection is larger in the present, developing flow. Figure 15 (*b*) again shows the energy balance at $x = 150$ mm, this time scaled by U_e and δ. Diffusion in a fully developed flow is always small in magnitude compared with the dissipation and production within the wall region, and any change in diffusion caused by a step change in roughness must be confined to the internal layer if $\overline{pv}$ is negligible. When longitudinal diffusion is small, that is when the thin shear layer approximation is valid (as it should be except very close to a step (Wood 1980)), it follows that

$$\int_0^{\delta_{i1}} D\,dy \simeq 0,$$

where D is the diffusion, if the *change* in diffusion caused by the change in boundary condition is large. The present results are generally consistent with this constraint. For similar reasons the large values of advection are contained within δ_{i1} at 150 mm.

At $x = 175$ mm the advection and production have decreased in magnitude as the

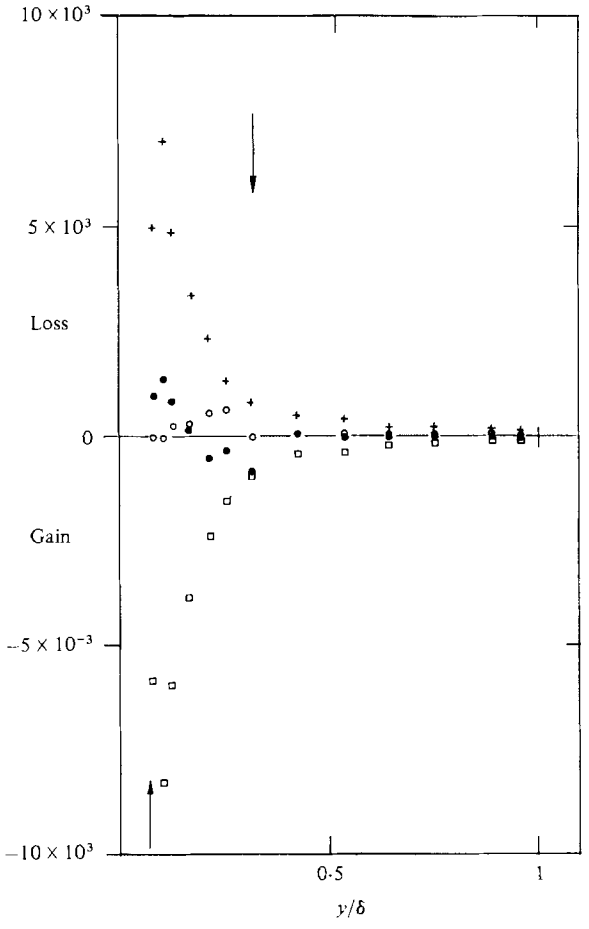

FIGURE 16. Turbulent-energy balance at $x = 175$ mm. Symbols as in figure 15 (*b*).

second internal layer is approached; the latter because although $-\overline{uv}$ has increased from 150 mm, $\partial U/\partial y$ has decreased more rapidly. Since the measured maxima for the second-order quantities occur at 175 mm the dominant contribution to the advection is $\frac{1}{2}V\partial\overline{q^2}/\partial y$ even though V is small. Within the second internal layer, $\partial U/\partial x > 0$, but it changes sign at $y = \delta_{i2}$, hence by continuity both V and the advection are zero just outside the second internal layer.

For $y < \delta_{i2}$ the rapid decrease in production and hence dissipation continues at $x = 200$ mm. The advection becomes a gain and reaches nearly 30 % of the production, compared with 50 % in the single $R \rightarrow S$ results of Antonia & Luxton (1972) at about one boundary-layer thickness from their step. As mentioned above, the perturbation as measured by M was larger in their case. At $x = 200$ mm the advection is dominated by $\frac{1}{2}U\partial\overline{q^2}/\partial x$, which changes sign just outside the second internal layer. The diffusion also changes sign near $y = \delta_{i2}$, and is positive in the outer part of the second internal layer, compared with the negative values near δ_{i1} at $x = 150$ mm. The behaviour of the diffusion is partially responsible for the slow growth of δ_{i2} in the outer layer. This can be shown qualitatively by noting that in the hyperbolic method of Bradshaw *et al.*

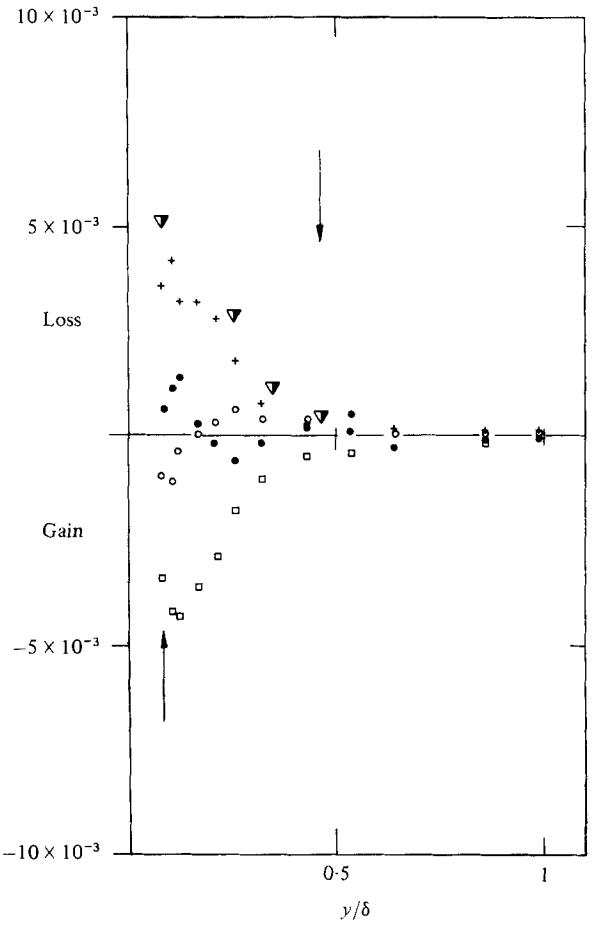

FIGURE 17. Turbulent-energy balance at $x = 200$ mm. Symbols as in figure 15 (*b*).

(1967) δ_{i2} can be identified with the outgoing characteristic originating at $x = 150$ mm, $y = 0$. From their equations

$$\frac{d\delta_{i2}}{dx} = \frac{V + \frac{1}{2}V_q + (\frac{1}{4}V_q^2 - 2a_1\overline{uv})^{\frac{1}{2}}}{U}, \tag{3.7}$$

where V_q is defined by (3.8) and the positive root is implied. The only approximation made in using (3.7) here is that the diffusion of turbulent energy is bulk convection by the large eddies. This assumption makes the Reynolds-stress transport equations hyperbolic. Within the wall region the right-hand side of (3.7) is dominated by $(-2a_1\overline{uv})^{\frac{1}{2}}U$, at least for single steps (Wood 1980) but the negative V_q for $y < \delta_{i2}$ (figure 19) must eventually reduce the growth of δ_{i2} in the outer layer.

Figure 18 shows the dissipation-length parameter $L_\epsilon \equiv (-\overline{uv})^{\frac{3}{2}}/\epsilon$, which characterizes the energy-containing eddies. Also shown is the equilibrium wall-region distribution $L_\epsilon = \kappa y$, and the distribution from Bradshaw *et al.* (1967) derived from fully developed flows. For $x > 150$ mm the implied increase from the equilibrium distribution is similar to the $R \rightarrow S$ measurements of Antonia & Luxton (1972). There is a plateau in L_ϵ outside the wall region for $y < \delta_{i2}$, and then L_ϵ rises until it reaches

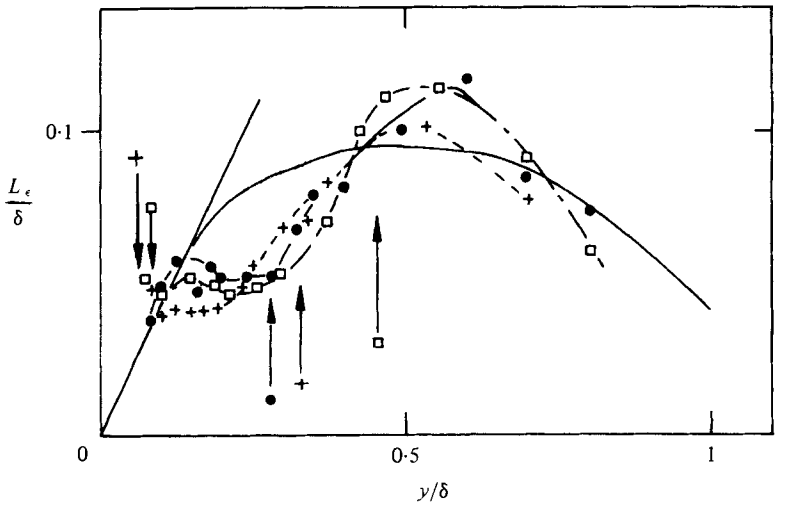

FIGURE 18. Dissipation-length parameter. Symbols as in figure 9. Downward-facing arrows show δ_{i2}/δ; upward-facing arrows, δ_{i1}/δ; ——, $L_\epsilon = \kappa y$ and distribution from Bradshaw *et al.* (1967).

approximately its fully developed value at around $y = \delta_{i1}$. Shear-stress balances are also shown in the report by Andreopoulos & Wood (1980).

It is often simpler to discuss the turbulent diffusion and transport in terms of the transport velocities

$$V_q \equiv (\overline{pv} + \tfrac{1}{2}\overline{q^2 v})/\tfrac{1}{2}\overline{q^2} \simeq \overline{q^2 v}/\overline{q^2} \equiv V'_q, \tag{3.8}$$

$$V_\tau \equiv (\overline{pu} + \overline{uv^2})/\overline{uv} \simeq \overline{uv^2}/\overline{uv} \equiv V'_\tau. \tag{3.9}$$

We emphasize that all the terms in the approximations V'_q and V'_τ were measured directly. V'_q is shown in figure 19 with the distribution used in the calculation method of Bradshaw *et al.* (1967), scaled appropriately for $x = 0$. Near the outer edge of a boundary layer V_q becomes constant and equal to $d(\delta - \delta^*)/dx$ as a consequence of the turbulent-energy equation reducing to Advection + Diffusion $\simeq 0$. V'_q is negative within the second internal layer; but as shown it is not zero where $\partial\overline{q^2}/\partial y$ is zero at $x = 200$ mm, as would be required by the gradient diffusion form $\overline{q^2 v} = C\,\partial\overline{q^2}/\partial y$, where C is the diffusivity. Andreopoulos & Bradshaw (1980) found that V_q was also negative very close to the surface in their fully developed rough-wall flow, indicating a transport of energy from the wall region towards the roughness elements, but it is unlikely that this mechanism is related to the present negative V'_q for $x > 150$ mm. The most striking feature of figure 19 is the outward propagation of the 'wave' in V_q after the roughness strip. The local maximum in V'_q occurs at $y/\delta = 0{\cdot}18$ for $x = 175$ mm and has moved out to $y/\delta = 0{\cdot}27$ at 250 mm. This behaviour is related directly to the stress bore first noted by Smits *et al.* (1979) downstream of an impulse of convex (stabilizing) curvature. Apart from the negative regions for $y < \delta_{i2}$, figure 19 is very similar to their figure 15(*d*). The present local maxima occur between δ_{i1} and δ_{i2} near the position where $\overline{q^2 v}$ is a maximum. Near the wall V'_τ (figure 20) is negative only for $x > 250$ mm. At 250 mm, V'_τ goes through zero close to where $-\overline{uv}$ is a maximum. Further downstream (the results are not shown here) the maximum in $-\overline{uv}$ moves slightly outward from the position where $V'_\tau = 0$. The ratio V'_q/V'_τ is generally about 3, as was found by Smits *et al.* (1979).

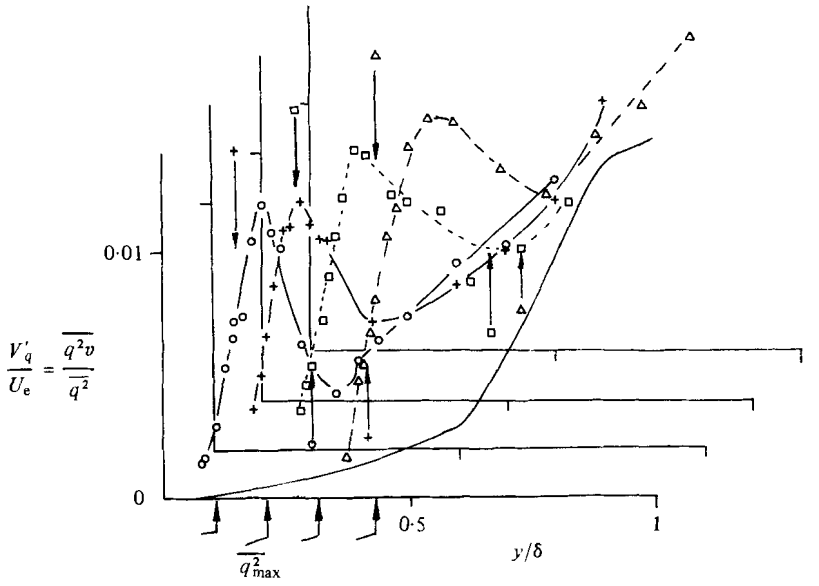

FIGURE 19. Profiles of V'_q/U_e. x (mm): ○, 150; +, 175; □, 200; △, 250. Solid line is distribution from Bradshaw *et al.* (1967), scaled for $x = 0$. Downward-facing arrows show δ_{i2}/δ. Upward-facing arrows *on figure* show δ_{i1}/δ. Upward-facing arrows *on bottom horizontal axis* show position of maximum $\overline{q^2}$.

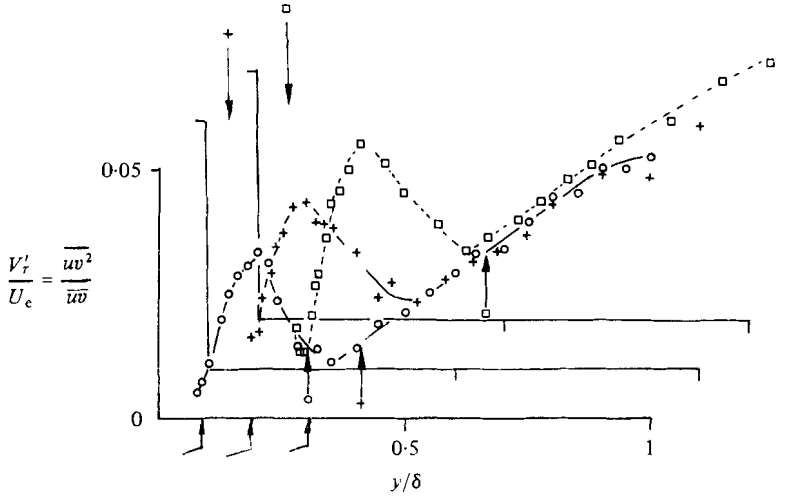

FIGURE 20. Profiles of V'_τ/U_e. Symbols as in figure 19. Arrows *on figure* as in figure 19. Upward-facing arrows *on bottom horizontal axis* show position of maximum $-\overline{uv}$.

4. Calculation of the flow

The method used was that of Bradshaw *et al.* (1967), which converts the turbulent-energy equation into an equation for $-\overline{uv}$. To do this, it was assumed that a_1 as defined here is 0·30, L_ϵ has the distribution shown in figure 18, and V_q has the distribution shown in figure 19. The calculations were started at $x = 0$ using the measured shear stress and mean-velocity profiles as input, and the rough surface was characterized by specifying $z_0 = 0{\cdot}134$ mm for $0 < x \leqslant 150$ mm. Details of the small, but necessary,

modifications made to the program described by Bradshaw & Unsworth (1974) are available from the second author.

The calculated values of c_f are shown in figure 2. The largest differences from the Clauser-chart values on the smooth wall occur close to the end of the roughness. Figure 21 compares the measured and calculated mean velocity and shear stress at $x = 200\,\text{mm}$; the largest discrepancies occur within the second internal layer for U/U_e and around $y/\delta = 0{\cdot}2$ for the shear stress. Figure 11 suggests that the measured a_1 does not depart sufficiently from 0·30 to cause serious errors, while figure 18 shows large deviations in L_ϵ from the assumed algebraic distribution. In principle, this defect can be overcome by using a transport equation for L_ϵ as was devised by Bradshaw & Unsworth (1974, 1976). Wood (1978) tested both the algebraic distribution and the transport equation for L_ϵ in the wall region after large $S \rightarrow R$ and $R \rightarrow S$ steps. The difference in the calculations was not large, especially compared with the departure of L_ϵ from the equilibrium distribution $L_\epsilon = \kappa y$ found by Antonia & Luxton (1971*a*, *b*, 1972) after large steps. This suggests that the major discrepancy between experiment and calculation is due to the behaviour of the diffusion term; in fact the regions of disagreement in figure 21 are centred first around the position where V_q goes through zero and then at the local maxima in V_q. Figure 22 shows the calculated and measured values of $y_{\tau\max}$ the position where $-\overline{uv}$ reaches its maximum. The calculated values near the step are always high, showing that the discrepancies apparent in figure 21 are general. The calculation method scales V_q by the maximum value of $-\overline{uv}$ for $y/\delta > 0{\cdot}25$, on the grounds that this is the representative turbulence-velocity scale in the outer layer. This is the reason for the behaviour of $y_{\tau\max}$ after $x = 350\,\text{mm}$; removing the restriction on locating the scale for V_q would increase the disparity between measured and calculated $y_{\tau\max}$ near the step.

The calculated c_f agrees very well with the Preston-tube measurements (figure 2). The most likely reason is that the usual logarithmic law (with $\Delta U/U_\tau = 0$) is used to calculate U_τ and U and $-\overline{uv}$ at the first mesh point, which corresponds to a y-value of between 1·25 mm (small x) and 2·88 mm.

5. General discussion and conclusions

The most obvious feature of the results is that the boundary layer has not recovered from the impulse of surface roughness within the measured range of x. At the last station, $x/\delta_0 = 55$, the additive constant in the logarithmic law is 7·0 and the shear-stress profile does not display standard smooth-wall behaviour (figure 5). The reason is contained in the mechanics of the stress bore and the consequent alteration principally to the turbulent diffusion (figure 19). This alteration probably caused most of the disagreement between the calculated and measured mean velocity and shear stress (figure 21). The long relaxation distance is similar to that implied by simpler $R \rightarrow S$ experiments, and is significantly longer than that for $S \rightarrow R$ steps. This can be explained qualitatively by noting that after a $R \rightarrow S$ step the outward propagation of the internal layer increases the shear stress towards the fully developed rough-wall distribution. After either a $R \rightarrow S$ step or an impulse of roughness the high level of shear stress in the outer layer must decay before full development is re-established.

The present flow is not a simple superposition of a $S \rightarrow R$ step followed quickly by a $R \rightarrow S$ step, as evidenced by the overshoot of the second-order products at $x = 175\,\text{mm}$

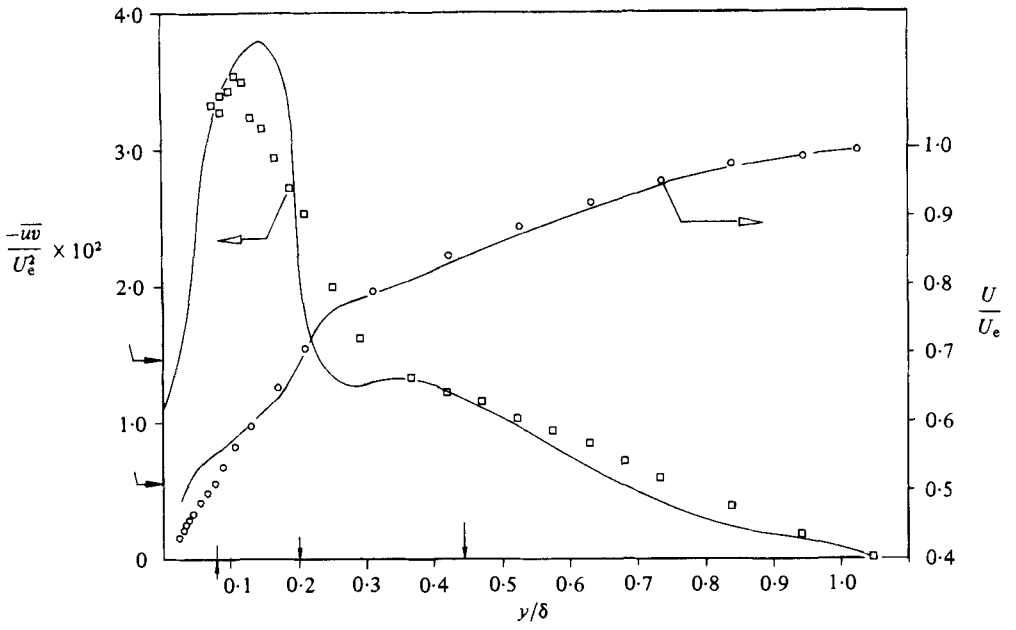

FIGURE 21. Calculated and measured mean velocity and shear stress at $x = 200$ mm. Wall shear stress from Clauser chart for $x = 0$, 200 mm is shown.

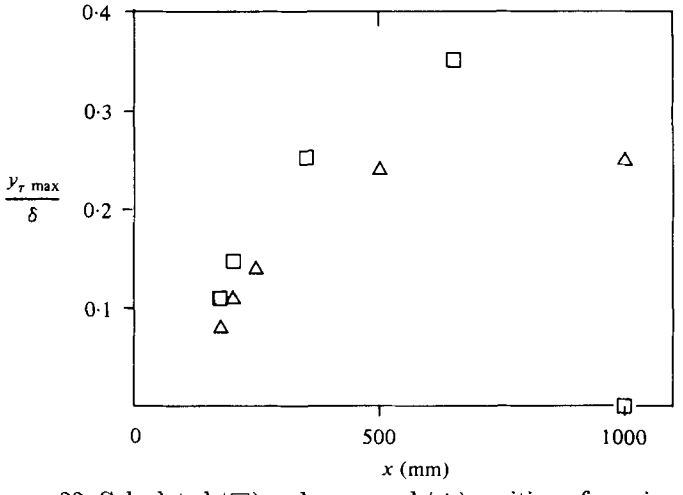

FIGURE 22. Calculated (□) and measured (△) position of maximum shear stress.

and by their maxima, at least for $x = 200$ mm, occurring outside the second internal layer. The negative V_q within the second internal layer is partially responsible for the slow rate of growth of δ_{i2} in the outer layer as given by (3.5) and (3.6). This negative region and the local maxima associated with the stress bore complicate the behaviour of V_q, but the results at face value imply a singularity in the gradient diffusion parameter $\overline{q^2 v}/\partial\overline{q^2}/\partial y$, where $\overline{q^2}$ is a maximum at $x = 200$ mm.

Within the wall region the growth of δ_{i2}, (3.4), agrees with the approximate correlation devised by Wood (1980) for single steps. This correlation implicitly ignores turbulent diffusion, as do the calculations of Wood (1978), also for single steps, leaving

the advection as the only important non-local term. In the present results, diffusion reaches 30% of the magnitude of the production near the wall, and so cannot be ignored in an improved description of the flow. A detailed explanation of why this occurs and how, for example, this alters the additive constant in the logarithmic law must await further investigation.

Our intellectual debt to Professor P. Bradshaw should be obvious. We are also grateful to him and to Professor W. Rodi for their comments on this work. J.A.'s contribution forms part of project A27 supported by Deutsche Forschungsgemeinschaft. At Imperial College, D.H.W. was supported by the Science Research Council and later by a Research Fellowship from the Australian Institute of Nuclear Science and Engineering.

REFERENCES

ANDREOPOULOS, J. 1979 *Univ. Karlsruhe Rep.* S.F.B. 80/E/149.

ANDREOPOULOS, J. 1980 *Univ. Karlsruhe Rep.* S.F.B. 80/E/181.

ANDREOPOULOS, J. 1981 Submitted to *J. Phys.* E: *Sci. Instr.*

ANDREOPOULOS, J. & BRADSHAW, P. 1981 *Boundary-Layer Met.* **20**, 201.

ANDREOPOULOS, J. & WOOD, D. H. 1980 *Univ. Karlsruhe Rep.* S.F.B. 80/E/180.

ANTONIA, R. A. & LUXTON, R. E. 1971*a* *J. Fluid Mech.* **48**, 721.

ANTONIA, R. A. & LUXTON, R. E. 1971*b* *Phys. Fluids* **14**, 1027.

ANTONIA, R. A. & LUXTON, R. E. 1972 *J. Fluid Mech.* **53**, 737.

ANTONIA, R. A. & LUXTON, R. E. 1974 *Adv. Geophys.* **18** A, 263.

BRADSHAW, P., FERRISS, B. H. & ATWELL, N. P. 1967 *J. Fluid Mech.* **28**, 593.

BRADSHAW, P. & UNSWORTH, K. 1974 *Imperial Coll. Aero. Rep.* no. 74-02.

BRADSHAW, P. & UNSWORTH, K. 1976 *Proc. Lockheed-Georgia Viscous Flow Symp., Lockheed-Georgia Co.* LG77ER044, p. 447.

ERMSHAUS, R. & NAUDASCHER, E. 1977 *Z. Flugwiss. Weltraumforschung* **1**, 419.

PATEL, V. C. 1965 *J. Fluid Mech.* **94**, 273.

PERRY, A. E., SCHOFIELD, W. H. & JOUBERT, P. N. 1969 *J. Fluid Mech.* **37**, 383.

SMITS, A. J., YOUNG, S. T. B. & BRADSHAW, P. 1979 *J. Fluid Mech.* **94**, 209.

TOWNSEND, A. A. 1961 *J. Fluid Mech.* **11**, 97.

TOWNSEND, A. A. 1976 *The Structure of Turbulent Shear Flow*, 2nd edn. Cambridge University Press.

WOOD, D. H. 1978 *Quart. J. R. Met. Soc.* **104**, 383.

WOOD, D. H. 1980 Internal layer growth following a step change in surface roughness. *Boundary-Layer Met.* (to be published).